CMS Physics Analysis Summary

Contact: cms-pag-conveners-heavyions@cern.ch 2024/06/02

Azimuthal dependence of hyperon polarization along the beam direction in pPb collisions at $\sqrt{s_{NN}}$ = 8.16 TeV

The CMS Collaboration

Abstract

The polarization of the Λ and $\overline{\Lambda}$ hyperons along the beam (z) direction, P_z, has been measured for the first time in pPb collisions at the LHC with $\sqrt{s_{NN}}$ = 8.16 TeV data collected by the CMS experiment. Assuming the largest contributions to P_z come from collective flow, this polarization can be characterized by the Fourier sine coefficients $P_{z,sn} = \langle P_z \sin(n\phi - n\Psi_n)\rangle$, where ϕ is the hyperon azimuthal emission angle and Ψ_n is the n-th order flow plane angle. The second order Fourier sine coefficient $P_{z,s2}$ is reported for Λ and $\overline{\Lambda}$ particles as a function of transverse momentum and event multiplicity. A significant positive $P_{z,s2}$ signal is observed for $0.8 < p_{\mathrm{T}} < 6.0$ GeV/c over the entire multiplicity range (from 3 to 250 charged particles). The measured $P_{z,s2}$ values increase as a function of p_{T} and decrease as a function of multiplicity. These results can provide new constraints on the potential creation of quark-gluon plasma droplets and the spin polarization mechanism in pp and pA systems.

Quantum chromodynamics (QCD) predicts that nuclear matter undergoes a phase transition to a deconfined partonic phase called the quark-gluon plasma (QGP) at very high density and temperature[1, 2]. This state of matter is generated in ultra-relativistic heavy nuclei collisions and behaves almost like an ideal fluid [3]. The non-trivial velocity and vorticity fields developed in the evolution of the QGP induce polarization of the produced particles via spin-orbit coupling [4–6], analogous to the Barnett effect [7, 8]. In particular, a net particle polarization along the orbital momentum of the colliding nuclei, referred to as global polarization, is generated by the non-zero vorticity component resulting from the shear in the initial velocity distributions of the participants in off-center nucleus-nucleus collisions. The observations of the Λ hyperon global polarization along the orbital momentum of the colliding nuclei in heavy-ion collisions at RHIC [9–11] and the LHC [12] open new directions in the study of the fluid and spin dynamics of QGP.

In nucleus-nucleus collisions, pressure gradients in the created QGP lead to azimuthally anisotropic particle emission, a phenomenon known as collective flow [13–15]. The collective flow generates non-zero vorticity along the beam (z) axis that, in turn, results in particle polarization along the beam direction (P_z) [16, 17]. This polarization, sometimes referred to as "local polarization" [18, 19], can be characterized by the Fourier sine coefficients $P_{z,sn} = \langle P_z \sin(n\phi - n\Psi_n)\rangle$, where ϕ is the hyperon azimuthal emission angle. The n-th order collective flow event plane angle Ψ_n is defined as $\frac{1}{n}\arctan\left(\frac{\sum_i \sin(n\phi_i)}{\sum_i \cos(n\phi_i)}\right)$, where ϕ_i is the azimuthal angle of the i^{th} emitted particle. The Λ hyperon P_z value with respect to the second-order event plane was first measured in gold-gold collisions at $\sqrt{s_{_{NN}}}$= 200 GeV [11] and later in lead-lead (PbPb) collisions at $\sqrt{s_{_{NN}}}$= 5.02 TeV [20]. Recently, similar polarization has been observed with respect to the third-order event plane in ruthenium-ruthenium and zirconian-zirconian collisions at $\sqrt{s_{_{NN}}}$= 200 GeV [21]. Within the frame of hydrodynamic and transport models, it has been found that the inclusion of the shear-induced polarization in addition to the thermal vorticity is required to capture the sign and magnitude of the data [17, 19, 22–26]. However, these calculations strongly depend on the implementation details of the shear contributions [26] and the shear-induced contribution may not be sufficient to fully understand the experimental results [27].

The general polarization of Λ hyperons produced in the high energy collisions of unpolarized hadrons has been a major challenge for QCD theoretical interpretations for several decades [28, 29]. Recently, the transverse polarization of Λ hyperons has been measured in unpolarized e^+e^- collisions by the Belle collaboration [30], with Polarizing Fragmentation Functions (PFFs) proposed as the origin of the measured polarization [31–39]. The potential dependence on the parton flavor [37], however, makes it unclear how PFFs contribute to Λ hyperon polarization in pPb collisions at LHC energies.

The observation of collective flow signals in events with high final-state particle multiplicity in proton-proton (pp) [40–45] and proton-lead (pPb) [46–52] collisions at the LHC, as well as at RHIC in proton-gold, deuteron-gold and helium-3–gold collisions [53–57], has raised the question whether a fluid-like QGP is created in these lighter hadronic collision systems. If such a medium is created in those collision systems, the azimuthal-dependent pressure gradients will lead to similar vorticity structures as in nucleus-nucleus collisions. It is of great interest to investigate whether such a complex vorticity is created in the small sized collisions by measuring Λ hyperon polarization along the beam direction. These results can provide stringent constraints on the thermal velocity and shear-induced contribution to the observed hyperon polarization in AA collisions. The Λ hyperon polarization measurements in pPb collisions can also shed light on the PFFs effects in various colliding systems.

This note presents first measurements of Λ and $\overline{\Lambda}$ hyperon polarization along the beam direc-

tion in pPb collisions at $\sqrt{s_{_{NN}}}$= 8.16 TeV. The second-order Fourier sine coefficients $P_{z,s2}$ of Λ and $\overline{\Lambda}$ particles with $|\eta| < 2.4$ and $0.8 < p_T < 6.0\,\text{GeV}/c$ are reported as functions of transverse momentum (p_T) and event multiplicity from 3 to 250.

The central feature of the CMS apparatus is a superconducting solenoid of 6 m internal diameter, providing a magnetic field of 3.8 T. Within the solenoid volume, there are four primary subdetectors including a silicon pixel and strip tracker detector, a lead tungstate crystal electromagnetic calorimeter, and a brass and scintillator hadron calorimeter, each composed of a barrel and two endcap sections. Iron and quartz-fiber Cherenkov hadron forward (HF) calorimeters cover the range $2.9 < |\eta| < 5.2$. The silicon tracker measures charged particles within the range $|\eta| < 2.5$. For charged particles with $1 < p_\text{T} < 10\,\text{GeV}/c$ and $|\eta| < 1.4$, the track resolutions are typically 1.5% in p_T and 25–90 (45–150) μm in the transverse (longitudinal) impact parameter [58]. A detailed description of the CMS detector, together with a definition of the coordinate system used and the relevant kinematic variables, can be found in Ref. [59].

The pPb data at $\sqrt{s_{_{NN}}} = 8.16$ TeV used in this analysis were collected by the CMS experiment in 2016, and correspond to an integrated luminosity of $186.0 \pm 6.5\,\text{nb}^{-1}$ [60]. The beam energies are 6.5 TeV for the protons and 2.56 TeV per nucleon for the lead nuclei. The event reconstruction, event selections, and triggers are identical to those described in Refs. [43, 61, 62]. The minimum bias (MB) events are triggered by requiring energy deposits above 1 GeV in at least one of the two HF calorimeters and the presence of at least one track with $p_\text{T} > 0.4\,\text{GeV}/c$ reconstructed using hits from the pixel tracker only. Dedicated high-multiplicity (HM) triggers are implemented to collect large samples of pPb collisions with large number of final state particles. The total number of combined ECAL and HCAL towers having deposited energy above a threshold of 0.5 GeV in transverse energy (E_T) is required to be greater than 120 and 150, while the number of reconstructed tracks by the high-level trigger [63, 64] with $|\eta| < 2.4$, $p_\text{T} > 0.4\,\text{GeV}/c$ are required to be greater or equal to 120, 150 and 185. The events are required to contain a primary vertex within 15 cm of the nominal interaction point along the beam axis and 0.2 cm in the transverse direction.

The pPb data are analyzed in several charged-particle multiplicity classes defined according to the number of selected primary tracks ($N_\text{trk}^\text{offline}$) with $|\eta| < 2.4$ and $p_\text{T} > 0.4\,\text{GeV}$ that originate from the primary vertex [43, 58]. Table 1 summaries the average number of tracks in pPb collisions, containing at least one reconstructed Λ or $\overline{\Lambda}$ candidate, in each $N_\text{trk}^\text{offline}$ range before and after correcting for inefficiencies and misidentification rates, denoted as $\langle N_\text{trk}^\text{offline}\rangle$ and $\langle N_\text{trk}^\text{corrected}\rangle$, respectively. The systematic uncertainty of $\langle N_\text{trk}^\text{corrected}\rangle$ is 4% resulting from the uncertainty of tracking efficiency estimated based on simulated events, while statistical uncertainty has been found to be negligible. Events with $N_\text{trk}^\text{offline} < 3$ are not included due to relatively low data taking efficiency, while events in the multiplicity region of $N_\text{trk}^\text{offline} > 250$ are not included to avoid effects of multiple interactions in a single event (pileup).

The reconstruction and selection procedures for strange hadron candidates in pPb collisions are identical to those in Refs. [43, 50, 65, 66]. Pairs of oppositely charged particle tracks with both transverse and longitudinal impact parameter significance greater than 1 with respect to the primary vertex are selected to determine if they point to a common secondary vertex resulting from the decay of a Λ candidate. The reconstruction efficiency for tracks with low momenta and large impact parameters is increased by using all tracks that pass the loose selection of Ref. [58]. The track pair is assumed to originate from $\pi^-\text{p}$ ($\pi^+\overline{\text{p}}$) in the Λ ($\overline{\Lambda}$) reconstruction.

Several topological selections are applied to further reduce the combinatorial background. The selection is optimized in order to maximize the statistical significance of the signal. In partic-

Table 1: The average multiplicity before (and after) corrections, $\langle N_{\mathrm{trk}}^{\mathrm{offline}} \rangle$ ($\langle N_{\mathrm{trk}}^{\mathrm{corrected}} \rangle$) with track $p_{\mathrm{T}} > 0.4\,\mathrm{GeV}$ and $|\eta_{\mathrm{lab}}| < 2.4$ in each multiplicity interval of pPb collisions containing at least one reconstructed Λ or $\overline{\Lambda}$ candidate. The uncertainties reported for $\langle N_{\mathrm{trk}}^{\mathrm{corrected}} \rangle$ are systematic uncertainties, as the statistical uncertainties have been found to be negligible.

Multiplicity interval ($N_{\mathrm{trk}}^{\mathrm{offline}}$)	$\langle N_{\mathrm{trk}}^{\mathrm{offline}} \rangle$	$\langle N_{\mathrm{trk}}^{\mathrm{corrected}} \rangle$
$[3, 60)$	40.0	48.5 ± 1.9
$[60, 120)$	86.7	105.3 ± 4.2
$[120, 150)$	132.7	161.2 ± 6.4
$[150, 185)$	163.6	198.7 ± 7.9
$[185, 250)$	203.3	246.9 ± 9.9

ular, strange hadron candidates are selected requiring the χ^2 probability of their decay vertex to be less than 7, the three-dimensional distance (normalized by its uncertainty) between the primary and secondary vertices to exceed 5, and the pointing angle (θ^{point}), defined as the angle between the line segment connecting the primary and decay vertices and the momentum vector of the reconstructed particle candidates in the plane transverse to the beam direction, to satisfy $\cos\theta^{\mathrm{point}} > 0.999$. These selections reduce the fraction of secondary Λ particles originating from the weak decays of Ξ^- and Ω^- particles to 10% and 1%, respectively. The limited number of detected Ξ^- and Ω^- particles does not allow for corresponding polarizations to be determined, preventing a correction due to these secondary Λ particles.

As the spin of a particle cannot be measured directly, the parity-violating weak decays of $\Lambda \to p + \pi^-$ and $\bar{\Lambda} \to \bar{p} + \pi^+$, in which the momentum direction of the daughter proton is correlated with the spin of the hyperon, are used to measure the polarization. The angular distribution of the proton in the hyperon rest frame is given by

$$\frac{dN}{d\Omega} \propto 1 + \alpha_\Lambda P_\Lambda \cos\theta^* \tag{1}$$

where α_Λ is the hyperon decay parameter ($\alpha_\Lambda = 0.750 \pm 0.009$, $\alpha_{\bar{\Lambda}} = -0.758 \pm 0.010$ [67]), P_Λ is the hyperon polarization, and θ^* is the angle between the polarization vector and the direction of the daughter baryon momentum in the hyperon rest frame. The polarization P_z can be estimated by averaging θ^* over all hyperons in collisions [11]:

$$P_z = \frac{\langle \cos\theta^* \rangle}{\alpha_\Lambda \langle \cos^2\theta^* \rangle}. \tag{2}$$

The factor $\langle \cos^2\theta^* \rangle$, which equals to 1/3 in the case of an ideal detector, is calculated directly from the data and found to range from 0.303 to 0.351.

The second-order Fourier sine coefficient, $P_{z,s2}$, can be measured directly as

$$\langle P_z \sin(2\phi - 2\Psi_2) \rangle = \frac{\langle \cos\theta^* \sin(2\phi - 2\Psi_2) \rangle}{\alpha_\Lambda Res(\Psi_2) \langle \cos^2\theta^* \rangle}, \tag{3}$$

where $Res(\Psi_2)$ is the event plane resolution. The event plane angle Ψ_2 is determined by the flow vector constructed from tracks within the transverse momentum range of $0.3 < p_{\mathrm{T}} < 3.0\,\mathrm{GeV}/c$ and $|\eta| < 2.4$. The two components of the second harmonic flow vector are given by:

$$Q_{2,x} = Q_2 \cos(2\Psi_2) = \sum_i \omega_i \cos(2\phi_i), Q_{2,y} = Q_2 \sin(2\Psi_2) = \sum_i \omega_i \sin(2\phi_i), \tag{4}$$

where ϕ_i are the azimuthal angles of the tracks and ω_i are the track p_{T} values. To compensate the imperfect detector acceptance, the flow vectors are re-centered by:

$$Q'_{2,x} = Q_{2,x} - \langle Q_{2,x} \rangle, \quad Q'_{2,y} = Q_{2,y} - \langle Q_{2,y} \rangle, \tag{5}$$

and Ψ_2 is estimated from the re-centered flow vector components as:

$$\Psi_2 = \frac{1}{2} \arctan\left(\frac{Q'_{2,y}}{Q'_{2,x}} \right). \tag{6}$$

Furthermore, a standard flattening technique is then used to remove the residual non-uniformities in the event plane angular distribution with $n_{max} = 10$ [68]. The event plane resolution $Res(\Psi_2)$ is estimated with the three-subevent method [69],

$$\langle \cos(2(\Psi_2^a - \Psi_2^R)) \rangle = \sqrt{\frac{\langle \cos(2(\Psi_2^a - \Psi_2^b)) \rangle \langle \cos(2(\Psi_2^a - \Psi_2^c)) \rangle}{\langle \cos(2(\Psi_2^b - \Psi_2^c)) \rangle}}. \tag{7}$$

The positive η side HF and negative η side HF are used to determine Ψ_2^b and Ψ_2^c where ϕ_i and ω_i in eq. 4 are the azimuthal angles of the calorimeter towers and the transverse energy deposited in them. $Res(\Psi_2)$ ranges from 0.415 to 0.684 from low to high multiplicity regions.

To extract the polarization of the hyperon signal, a simultaneous fit to the invariant mass spectrum of hyperon candidates and their $\langle P_z \sin(2\phi - 2\Psi_2) \rangle$ values as a function of invariant mass is performed. The mass spectrum fit function is composed of the sum of two Gaussian functions with the same mean but different widths for the hyperon signal, $S(m_{inv})$, and a function $Aq^{1/2} + Bq^{3/2}$, where $q = m - (m_\pi + m_p)$ and A, B are the fitted parameters, to model the combinatorial background, $B(m_{inv})$. The $\langle P_z \sin(2\phi - 2\Psi_2) \rangle$ distribution is fitted with

$$\begin{aligned} \langle \cos\theta^* \sin(2\phi - 2\Psi_2) \rangle^{S+B} = {} & \alpha(m_{inv}) \langle \cos\theta^* \sin(2\phi - 2\Psi_2) \rangle^S \\ & + [1 - \alpha(m_{inv})] \langle \cos\theta^* \sin(2\phi - 2\Psi_2) \rangle^B. \end{aligned} \tag{8}$$

Here $\langle \cos\theta^* \sin(2\phi - 2\Psi_2) \rangle^B$ for the background candidates is modeled as a linear function of the invariant mass, and $\alpha(m_{inv})$ is the hyperon signal fraction. Figure 1 shows an example of a simultaneous fit to the mass spectrum and $\langle \cos\theta^* \sin(2\phi - 2\Psi_2) \rangle^{S+B}$ for the multiplicity range $185 \leq N_{\mathrm{trk}}^{\mathrm{offline}} < 250$.

The sources of systematic uncertainty in the $P_{z,s2}$ measurement in this analysis include the variation of the background probability density function (PDF) for invariant mass and for the $\langle \cos\theta^* \sin(2\phi - 2\Psi_2) \rangle$ value of background Λ candidates, the vertex z-position selected range (v_z), the beam direction comparison, and the uncertainty on the hyperon decay parameter [67]. Systematic effects related to background invariant mass PDF are investigated by changing the PDF to 3rd order polynomial, exponential, 2nd order Chebyshev polynomial and 3rd order Chebyshev polynomial functions. A variation of 3% is found for all $P_{z,s2}$ results. The systematic uncertainties from the background $\langle \cos\theta^* \sin(2\phi - 2\Psi_2) \rangle$ functional form are evaluated by changing from linear function to a constant or fixed at 0. For $3 \leq N_{\mathrm{trk}}^{\mathrm{offline}} < 60$ and $60 \leq N_{\mathrm{trk}}^{\mathrm{offline}} < 120$, a systematic uncertainty of 3%(7%) is quoted for Λ ($\overline{\Lambda}$) results and 5% for Λ + $\overline{\Lambda}$ results, while the results are consistent in higher multiplicity ranges. To evaluate the uncertainties from detector acceptance, the $P_{z,s2}$ are extracted from events with $|v_z| < 3\,\mathrm{cm}$ and $3 < |v_z| < 15\,\mathrm{cm}$. A variation of 8% (3%) is found for $\Lambda/\overline{\Lambda}$ (Λ + $\overline{\Lambda}$) results which is quoted as systematic uncertainty. The beam direction has been reversed during the 2016 pPb collision data taking, and a systematic uncertainty of 10% is found by comparing results from

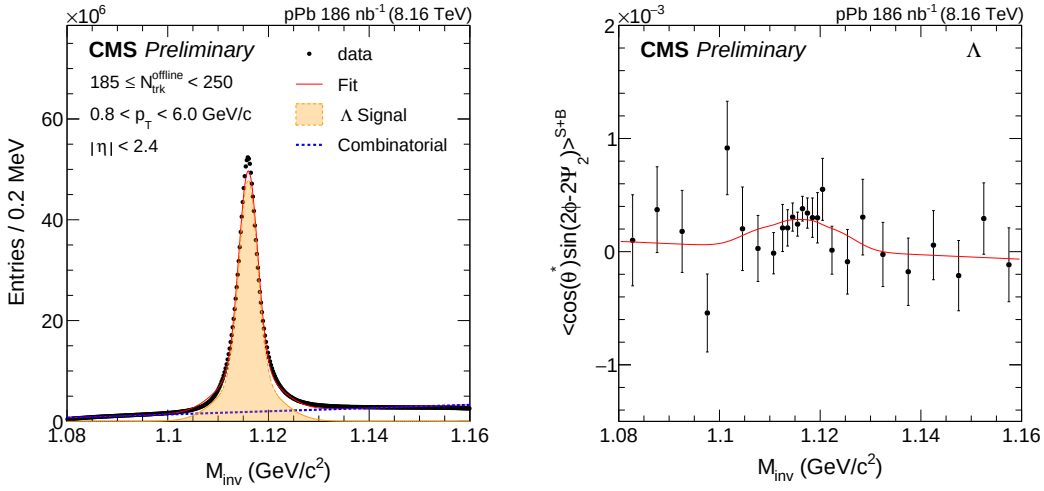

Figure 1: Example of the simultaneous fit to the mass spectrum and $\langle \cos\theta^* \sin(2\phi - 2\Psi_2)\rangle^{S+B}$ for the multiplicity range $185 \leq N_{\rm trk}^{\rm offline} < 250$. Vertical bars show the statistical uncertainties.

the two beam directions. The hyperon decay parameter measurements have their own uncertainties which transfer into global systematic uncertainties of 1.2% (1.3%) for Λ ($\overline{\Lambda}$) results and 1.3% for Λ + $\overline{\Lambda}$ results. To test the procedure of extracting the signal $P_{z,s2}$, a study using EPOS LHC [70] pPb events is performed and the extracted values are found to be consistent with the generator-level values.

Figure 2 shows the $N_{\rm trk}^{\rm offline}$ dependence of the second-order sine Fourier coefficients of polarization along the beam direction, $P_{z,s2}$, in pPb collisions at $\sqrt{s_{NN}}$= 8.16 TeV for Λ, $\overline{\Lambda}$ and Λ + $\overline{\Lambda}$. Significant positive $P_{z,s2}$ has been observed for the entire measured multiplicity range from 3 to 250. The $P_{z,s2}$ values for Λ and $\overline{\Lambda}$ particles are consistent with each other within uncertainties and found to decrease as a function of multiplicity. A similar trend has been observed in AA collisions where $P_{z,s2}$ increases from central to peripheral collisions [11, 20, 21]. The same measurement has been performed for K_S^0 particles following the same analysis procedure where the results are consistent with 0 as expected because K_S^0 is a spin 0 particle. The $P_{z,s2}$ results from EPOS LHC [70] simulations are shown in Fig.2. This Monte Carlo event generator models the particle production and collective flow without any polarization mechanism. The generator level (GEN) Λ and $\overline{\Lambda}$ particles and event plane reconstructed from charged GEN particles with identical kinematic selections to the data are used in the measurements, while the $N_{\rm trk}^{\rm offline}$ values are determined from the reconstructed tracks. A negative signal has been observed at low multiplicity region. Although the statistical uncertainties do not allow a solid conclusion, the $P_{z,s2}$ values tend to converge to 0 towards higher multiplicity.

The $P_{z,s2}$ results for Λ + $\overline{\Lambda}$ particles as functions of $p_{\rm T}$ for $3 \leq N_{\rm trk}^{\rm offline} < 60$, $60 \leq N_{\rm trk}^{\rm offline} < 120$ and $185 \leq N_{\rm trk}^{\rm offline} < 250$ are shown in Fig.3. The limited number of events collected for the $120 \leq N_{\rm trk}^{\rm offline} < 185$ region prevented a corresponding $P_{z,s2}$ result. An increasing trend as function of $p_{\rm T}$ is observed for all measured multiplicity ranges. The $p_{\rm T}$-dependence of $P_{z,s2}$ results tends to follow the trend of the 2nd order collective flow (v_2) in pPb collisions [51]. However, the increasing trend of $P_{z,s2}$ towards low multiplicity does not follow the multiplicity dependence of the v_2 values, similar to the observation in peripheral AA collisions [21]. It remains to be seen if the observed Λ hyperon polarization in pPb collisions and peripheral AA collisions is generated by a complex vorticity structure due to anisotropic expansion of the fluid-like QGP medium. In addition, how the PFFs effects, with a potential parton flavor

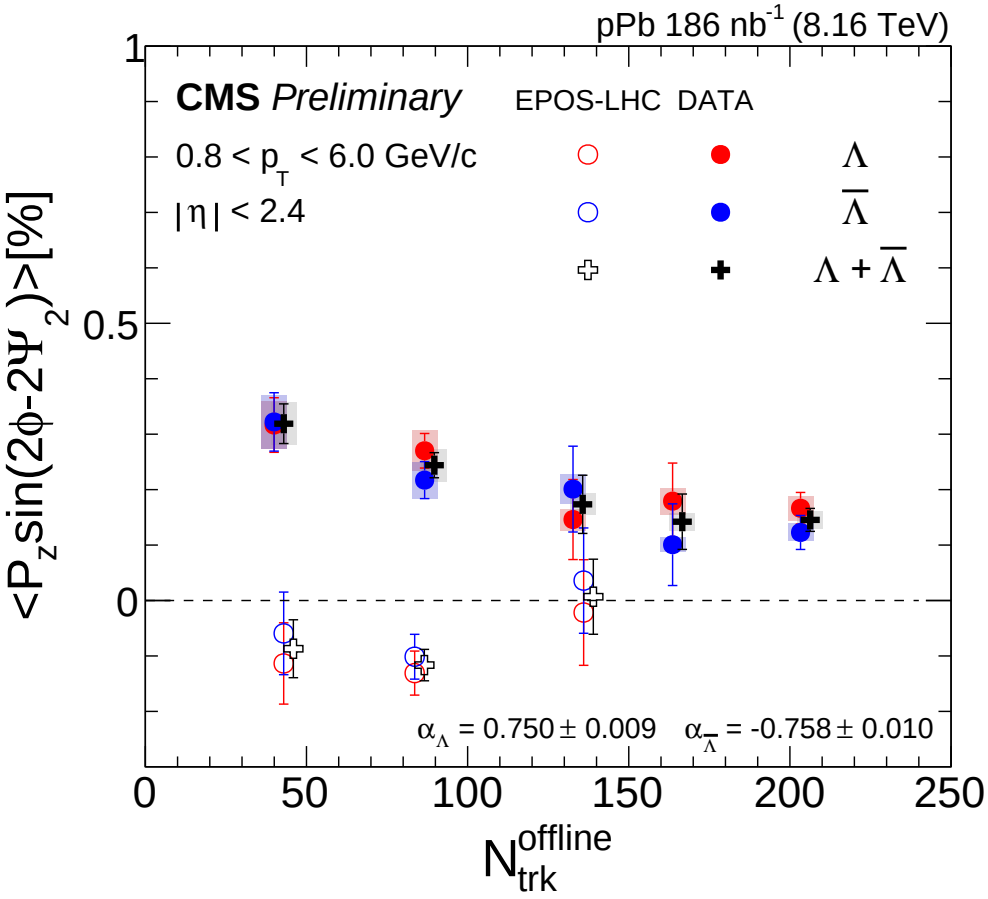

Figure 2: The second-order Fourier sine coefficients of Λ, $\overline{\Lambda}$ and $\Lambda + \overline{\Lambda}$ polarization along the beam direction as functions of $N_{\mathrm{trk}}^{\mathrm{offline}}$ in pPb collisions at $\sqrt{s_{NN}}$= 8.16 TeV. Results from EPOS LHC simulations are shown as hollow markers. Vertical bars present statistical uncertainties in both the measurements and the simulations. Shaded areas show systematic uncertainties in the measurements. The $N_{\mathrm{trk}}^{\mathrm{offline}}$ values of $\Lambda + \overline{\Lambda}$ results are shifted for better visibility.

dependence [37], contribute to the measured polarization in pPb collisions at the LHC energies need to be understood.

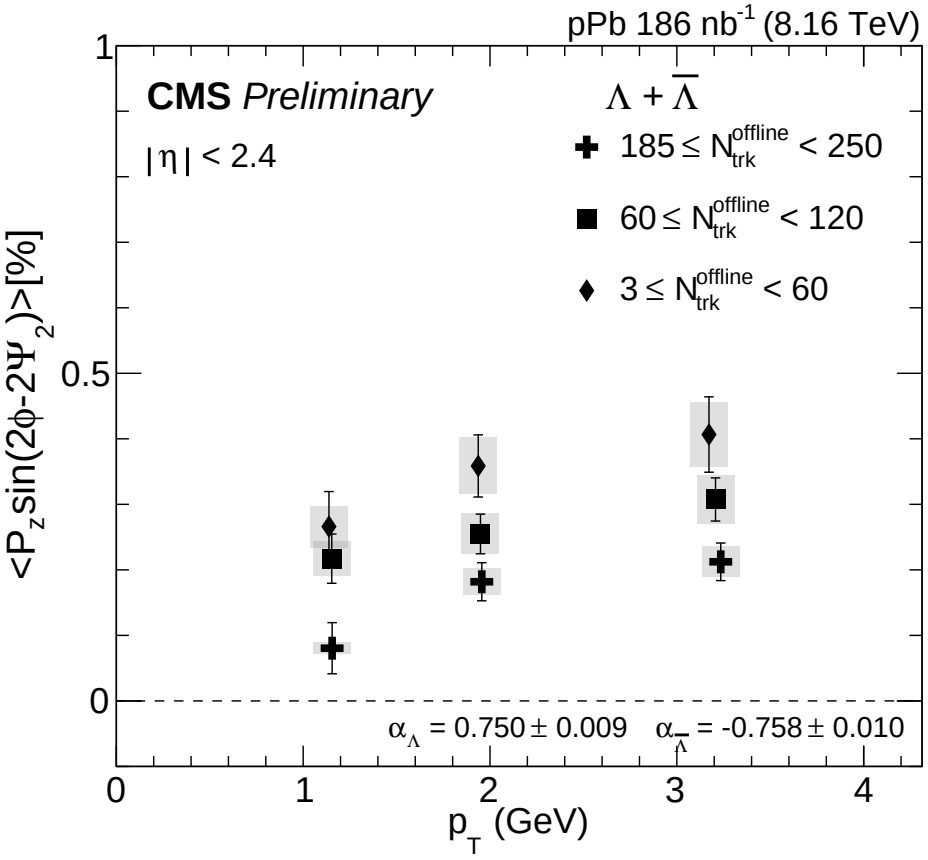

Figure 3: The second-order Fourier sine coefficients of $\Lambda + \overline{\Lambda}$ polarization along the beam direction as functions of p_{T} in pPb collisions at $\sqrt{s_{NN}}$= 8.16 TeV with $3 \leq N_{\mathrm{trk}}^{\mathrm{offline}} < 60$, $60 \leq N_{\mathrm{trk}}^{\mathrm{offline}} < 120$ and $185 \leq N_{\mathrm{trk}}^{\mathrm{offline}} < 250$. Vertical bars show statistical uncertainties. Shaded areas show systematic uncertainties.

In summary, the first measurements of the second-order sine Fourier coefficients $P_{z,s2}$ of hyperon polarization along the beam direction in proton-lead (pPb) collisions at $\sqrt{s_{NN}}$= 8.16 TeV as functions of multiplicity and transverse momentum are presented. Significant positive $P_{z,s2}$ values are observed for Λ and $\overline{\Lambda}$ particles over the entire multiplicity range from 3 to 250. An increasing trend with transverse momentum is observed for $P_{z,s2}$, while the values decrease with increasing particle multiplicity. The p_{T}-dependence of $P_{z,s2}$ measurements tends to follow the trend of the second-order collective flow in pPb collisions, while the multiplicity dependence does not. The observed signal might indicate that besides the complex vorticity structures due to expansion of the fluid-like QGP medium, alternative physics mechanisms such as the Polarizing Fragmentation Functions effects may contribute to the hyperon polarization along the beam direction in pPb collisions.

References

[1] E. V. Shuryak, "Theory of hadronic plasma", *Sov. Phys. JETP* **47** (1978) 212–219.

[2] J. C. Collins and M. J. Perry, "Superdense matter: neutrons or asymptotically free quarks?", *Phys. Rev. Lett.* **34** (1975) 1353, doi:10.1103/PhysRevLett.34.1353.

[3] P. Braun-Munzinger, V. Koch, T. Schäfer, and J. Stachel, "Properties of hot and dense matter from relativistic heavy ion collisions", *Phys. Rept.* **621** (2016) 76–126, doi:10.1016/j.physrep.2015.12.003, arXiv:1510.00442.

[4] Z.-T. Liang and X.-N. Wang, "Globally polarized quark-gluon plasma in non-central A+A collisions", *Phys. Rev. Lett.* **94** (2005) 102301, doi:10.1103/PhysRevLett.94.102301, arXiv:nucl-th/0410079. [Erratum: Phys.Rev.Lett. 96, 039901 (2006)].

[5] S. A. Voloshin, "Polarized secondary particles in unpolarized high energy hadron-hadron collisions?", arXiv:nucl-th/0410089.

[6] F. Becattini, F. Piccinini, and J. Rizzo, "Angular momentum conservation in heavy ion collisions at very high energy", *Phys. Rev. C* **77** (2008) 024906, doi:10.1103/PhysRevC.77.024906, arXiv:0711.1253.

[7] S. J. Barnett, "Magnetization by rotation", *Phys. Rev.* **6** (1915), no. 4, 239, doi:10.1103/PhysRev.6.239.

[8] S. J. Barnett, "Gyromagnetic and electron-inertia effects", *Rev. Mod. Phys.* **7** (1935), no. 2, 129, doi:10.1103/RevModPhys.7.129.

[9] STAR Collaboration, "Global Λ hyperon polarization in nuclear collisions: evidence for the most vortical fluid", *Nature* **548** (2017) 62–65, doi:10.1038/nature23004, arXiv:1701.06657.

[10] STAR Collaboration, "Global polarization of Λ hyperons in Au+Au collisions at $\sqrt{s_{NN}}$ = 200 GeV", *Phys. Rev. C* **98** (2018) 014910, doi:10.1103/PhysRevC.98.014910, arXiv:1805.04400.

[11] STAR Collaboration, "Polarization of Λ ($\bar{\Lambda}$) hyperons along the beam direction in Au+Au collisions at $\sqrt{s_{NN}}$ = 200 GeV", *Phys. Rev. Lett.* **123** (2019), no. 13, 132301, doi:10.1103/PhysRevLett.123.132301, arXiv:1905.11917.

[12] ALICE Collaboration, "Global polarization of $\Lambda\bar{\Lambda}$ hyperons in Pb-Pb collisions at $\sqrt{s_{NN}}$ = 2.76 and 5.02 TeV", *Phys. Rev. C* **101** (2020), no. 4, 044611, doi:10.1103/PhysRevC.101.044611, arXiv:1909.01281. [Erratum: Phys.Rev.C 105, 029902 (2022)].

[13] J.-Y. Ollitrault, "Anisotropy as a signature of transverse collective flow", *Phys. Rev. D* **46** (1992) 229, doi:10.1103/PhysRevD.46.229.

[14] U. Heinz and R. Snellings, "Collective flow and viscosity in relativistic heavy-ion collisions", *Ann. Rev. Nucl. Part. Sci.* **63** (2013) 123, doi:10.1146/annurev-nucl-102212-170540, arXiv:1301.2826.

[15] C. Gale, S. Jeon, and B. Schenke, "Hydrodynamic modeling of heavy-Ion collisions", *Int. J. Mod. Phys. A* **28** (2013) 1340011, doi:10.1142/S0217751X13400113, arXiv:1301.5893.

[16] S. A. Voloshin, "Vorticity and particle polarization in heavy ion collisions (experimental perspective)", *EPJ Web Conf.* **171** (2018) 07002, doi:10.1051/epjconf/201817107002, arXiv:1710.08934.

[17] F. Becattini and I. Karpenko, "Collective longitudinal polarization in relativistic heavy-Ion collisions at very high energy", *Phys. Rev. Lett.* **120** (2018), no. 1, 012302, doi:10.1103/PhysRevLett.120.012302, arXiv:1707.07984.

[18] J.-H. Gao et al., "Chiral anomaly and local polarization effect from quantum kinetic approach", *Phys. Rev. Lett.* **109** (2012) 232301, doi:10.1103/PhysRevLett.109.232301, arXiv:1203.0725.

[19] X.-L. Xia, H. Li, Z.-B. Tang, and Q. Wang, "Probing vorticity structure in heavy-ion collisions by local Λ polarization", *Phys. Rev. C* **98** (2018) 024905, doi:10.1103/PhysRevC.98.024905, arXiv:1803.00867.

[20] ALICE Collaboration, "Polarization of Λ and $\bar{\Lambda}$ hyperons along the beam direction in Pb-Pb collisions at $\sqrt{s_{NN}}$=5.02 TeV", *Phys. Rev. Lett.* **128** (2022), no. 17, 172005, doi:10.1103/PhysRevLett.128.172005, arXiv:2107.11183.

[21] STAR Collaboration, "Hyperon polarization along the beam direction relative to the second and third harmonic event planes in isobar collisions at sNN=200 GeV", *Phys. Rev. Lett.* **131** (2023), no. 20, 202301, doi:10.1103/PhysRevLett.131.202301, arXiv:2303.09074.

[22] B. Fu, K. Xu, X.-G. Huang, and H. Song, "Hydrodynamic study of hyperon spin polarization in relativistic heavy ion collisions", *Phys. Rev. C* **103** (2021), no. 2, 024903, doi:10.1103/PhysRevC.103.024903, arXiv:2011.03740.

[23] W. Florkowski, A. Kumar, R. Ryblewski, and A. Mazeliauskas, "Longitudinal spin polarization in a thermal model", *Phys. Rev. C* **100** (2019), no. 5, 054907, doi:10.1103/PhysRevC.100.054907, arXiv:1904.00002.

[24] B. Fu et al., "Shear-induced spin polarization in heavy-Ion collisions", *Phys. Rev. Lett.* **127** (2021), no. 14, 142301, doi:10.1103/PhysRevLett.127.142301, arXiv:2103.10403.

[25] F. Becattini et al., "Local polarization and isothermal local equilibrium in relativistic heavy ion collisions", *Phys. Rev. Lett.* **127** (2021), no. 27, 272302, doi:10.1103/PhysRevLett.127.272302, arXiv:2103.14621.

[26] S. Alzhrani, S. Ryu, and C. Shen, "Λ spin polarization in event-by-event relativistic heavy-ion collisions", *Phys. Rev. C* **106** (2022), no. 1, 014905, doi:10.1103/PhysRevC.106.014905, arXiv:2203.15718.

[27] W. Florkowski, A. Kumar, A. Mazeliauskas, and R. Ryblewski, "Effect of thermal shear on longitudinal spin polarization in a thermal model", *Phys. Rev. C* **105** (2022), no. 6, 064901, doi:10.1103/PhysRevC.105.064901, arXiv:2112.02799.

[28] G. Bunce et al., "Lambda hyperon polarization in inclusive production by 300-GeV protons on beryllium.", *Phys. Rev. Lett.* **36** (1976) 1113–1116, doi:10.1103/PhysRevLett.36.1113.

[29] K. J. Heller et al., "Polarization of lambdas and anti-lambdas produced by 400-GeV protons", *Phys. Rev. Lett.* **41** (1978) 607, doi:10.1103/PhysRevLett.41.607. [Erratum: Phys.Rev.Lett. 45, 1043 (1980)].

[30] Belle Collaboration, "Observation of transverse $\Lambda/\bar{\Lambda}$ hyperon polarization in e^+e^- annihilation at Belle", *Phys. Rev. Lett.* **122** (2019), no. 4, 042001, doi:10.1103/PhysRevLett.122.042001, arXiv:1808.05000.

[31] M. Anselmino, R. Kishore, and A. Mukherjee, "Polarizing fragmentation function and the Λ polarization in e^+e^- processes", *Phys. Rev. D* **100** (2019), no. 1, 014029, doi:10.1103/PhysRevD.100.014029, arXiv:1905.02777.

[32] U. D'Alesio, F. Murgia, and M. Zaccheddu, "First extraction of the Λ polarizing fragmentation function from Belle e^+e^- data", *Phys. Rev. D* **102** (2020), no. 5, 054001, doi:10.1103/PhysRevD.102.054001, arXiv:2003.01128.

[33] D. Callos, Z.-B. Kang, and J. Terry, "Extracting the transverse momentum dependent polarizing fragmentation functions", *Phys. Rev. D* **102** (2020), no. 9, 096007, doi:10.1103/PhysRevD.102.096007, arXiv:2003.04828.

[34] K.-B. Chen et al., "Isospin symmetry of fragmentation functions", *Phys. Lett. B* **816** (2021) 136217, doi:10.1016/j.physletb.2021.136217, arXiv:2102.00658.

[35] H. Li, X. Wang, Y. Yang, and Z. Lu, "The transverse polarization of Λ hyperons in $e^+e^- \to \Lambda^\uparrow hX$ processes within TMD factorization", *Eur. Phys. J. C* **81** (2021), no. 4, 289, doi:10.1140/epjc/s10052-021-09064-1, arXiv:2009.07193.

[36] L. Gamberg et al., "Polarized hyperon production in single-inclusive electron-positron annihilation at next-to-leading order", *JHEP* **01** (2019) 111, doi:10.1007/JHEP01(2019)111, arXiv:1810.08645.

[37] L. Gamberg et al., "Transverse Λ polarization in e^+e^- collisions", *Phys. Lett. B* **818** (2021) 136371, doi:10.1016/j.physletb.2021.136371, arXiv:2102.05553.

[38] Y. Yang, X. Wang, and Z. Lu, "Predicting the $\sin\phi_S$ single-spin-asymmetry of Λ production off transversely polarized nucleon in SIDIS", *Phys. Rev. D* **103** (2021) 114011, doi:10.1103/PhysRevD.103.114011, arXiv:2103.11348.

[39] H. Li, X. Wang, and Z. Lu, "sin($\phi\Lambda$-ϕS) azimuthal asymmetry in transversely polarized Λ production in SIDIS within TMD factorization at the EIC", *Phys. Rev. D* **104** (2021), no. 3, 034020, doi:10.1103/PhysRevD.104.034020, arXiv:2104.12155.

[40] CMS Collaboration, "Observation of long-range near-side angular correlations in proton-proton collisions at the LHC", *JHEP* **09** (2010) 091, doi:10.1007/JHEP09(2010)091, arXiv:1009.4122.

[41] ATLAS Collaboration, "Observation of long-range elliptic anisotropies in $\sqrt{s}$ =13 and 2.76 TeV pp collisions with the ATLAS detector", arXiv:1509.04776.

[42] CMS Collaboration, "Measurement of long-range near-side two-particle angular correlations in pp collisions at $\sqrt{s}$ =13 TeV", *Phys. Rev. Lett.* **116** (2016), no. 17, 172302, doi:10.1103/PhysRevLett.116.172302, arXiv:1510.03068.

[43] CMS Collaboration, "Evidence for collectivity in pp collisions at the LHC", *Phys. Lett.* **B765** (2017) 193–220, doi:10.1016/j.physletb.2016.12.009, arXiv:1606.06198.

[44] CMS Collaboration, "Evidence for collectivity in pp collisions at the LHC", *Phys. Lett. B* **765** (2017) 193–220, doi:10.1016/j.physletb.2016.12.009, arXiv:1606.06198.

[45] CMS Collaboration, "Studies of charm and beauty hadron long-range correlations in pp and pPb collisions at LHC energies", *Phys. Lett. B* **813** (2021) 136036, doi:10.1016/j.physletb.2020.136036, arXiv:2009.07065.

[46] CMS Collaboration, "Observation of long-range near-side angular correlations in proton-lead collisions at the LHC", *Phys. Lett. B* **718** (2013) 795, doi:10.1016/j.physletb.2012.11.025, arXiv:1210.5482.

[47] ALICE Collaboration, "Long-range angular correlations on the near and away side in pPb collisions at $\sqrt{s_{_{NN}}}$ = 5.02 TeV", *Phys. Lett. B* **719** (2013) 29, doi:10.1016/j.physletb.2013.01.012, arXiv:1212.2001.

[48] ATLAS Collaboration, "Observation of associated near-side and away-side long-range correlations in $\sqrt{s_{NN}} = 5.02$ TeV proton-lead collisions with the ATLAS detector", *Phys. Rev. Lett.* **110** (2013) 182302, doi:10.1103/PhysRevLett.110.182302, arXiv:1212.5198.

[49] LHCb Collaboration, "Measurements of long-range near-side angular correlations in $\sqrt{s_{\rm NN}} = 5$TeV proton-lead collisions in the forward region", arXiv:1512.00439.

[50] CMS Collaboration, "Elliptic flow of charm and strange hadrons in high-multiplicity pPb collisions at $\sqrt{s_{_{\rm NN}}} = 8.16$ TeV", *Phys. Rev. Lett.* **121** (2018), no. 8, 082301, doi:10.1103/PhysRevLett.121.082301, arXiv:1804.09767.

[51] CMS Collaboration, "Observation of prompt J/ψ meson elliptic flow in high-multiplicity pPb collisions at $\sqrt{s_{\rm NN}} = 8.16$ TeV", *Phys. Lett. B* **791** (2019) 172–194, doi:10.1016/j.physletb.2019.02.018, arXiv:1810.01473.

[52] CMS Collaboration, "Strange hadron collectivity in pPb and PbPb collisions", *JHEP* **05** (2023) 007, doi:10.1007/JHEP05(2023)007, arXiv:2205.00080.

[53] PHENIX Collaboration, "Measurement of long-range angular correlation and quadrupole anisotropy of pions and (anti)protons in central d+Au collisions at $\sqrt{s_{_{NN}}}$ = 200 GeV", *Phys. Rev. Lett.* **114** (2015) 192301, doi:10.1103/PhysRevLett.114.192301, arXiv:1404.7461.

[54] STAR Collaboration, "Long-range pseudorapidity dihadron correlations in d+Au collisions at $\sqrt{s_{\rm NN}} = 200$ GeV", *Phys. Lett.* **B747** (2015) 265–271, doi:10.1016/j.physletb.2015.05.075, arXiv:1502.07652.

[55] PHENIX Collaboration, "Measurements of elliptic and triangular flow in high-multiplicity ^{3}He+Au collisions at $\sqrt{s_{_{NN}}}$ = 200 GeV", *Phys. Rev. Lett.* **115** (2015) 142301, doi:10.1103/PhysRevLett.115.142301, arXiv:1507.06273.

[56] PHENIX Collaboration, "Creation of quark–gluon plasma droplets with three distinct geometries", *Nature Phys.* **15** (2019), no. 3, 214–220, doi:10.1038/s41567-018-0360-0, arXiv:1805.02973.

[57] STAR Collaboration, "Measurements of the elliptic and triangular azimuthal anisotropies in central He3+Au, d+Au and p+Au collisions at sNN=200 GeV", *Phys. Rev. Lett.* **130** (2023), no. 24, 242301, doi:10.1103/PhysRevLett.130.242301, arXiv:2210.11352.

[58] CMS Collaboration, "Description and performance of track and primary-vertex reconstruction with the CMS tracker", *JINST* **9** (2014), no. 10, P10009, doi:10.1088/1748-0221/9/10/P10009, arXiv:1405.6569.

[59] CMS Collaboration, "The CMS experiment at the CERN LHC", *JINST* **3** (2008) S08004, doi:10.1088/1748-0221/3/08/S08004.

[60] CMS Collaboration, "CMS luminosity measurement using 2016 proton-nucleus collisions at $\sqrt{s_{_{\mathrm{NN}}}} = 8.16\,\mathrm{TeV}$", CMS Physics Analysis Summary CMS-PAS-LUM-17-002, 2018.

[61] CMS Collaboration, "Constraints on the chiral magnetic effect using charge-dependent azimuthal correlations in *p*Pb and PbPb collisions at the CERN Large Hadron Collider", *Phys. Rev. C* **97** (2018), no. 4, 044912, doi:10.1103/PhysRevC.97.044912, arXiv:1708.01602.

[62] CMS Collaboration, "Observation of correlated azimuthal anisotropy fourier harmonics in pp and p+Pb collisions at the LHC", *Phys. Rev. Lett.* **120** (2018) 092301, doi:10.1103/PhysRevLett.120.092301, arXiv:1709.09189.

[63] CMS Collaboration, "Performance of the CMS Level-1 trigger in proton-proton collisions at $\sqrt{s} = 13$ TeV", *JINST* **15** (2020), no. 10, P10017, doi:10.1088/1748-0221/15/10/P10017, arXiv:2006.10165.

[64] CMS Collaboration, "The CMS trigger system", *JINST* **12** (2017), no. 01, P01020, doi:10.1088/1748-0221/12/01/P01020, arXiv:1609.02366.

[65] CMS Collaboration, "Long-range two-particle correlations of strange hadrons with charged particles in pPb and PbPb collisions at LHC energies", *Phys. Lett. B* **742** (2015) 200, doi:10.1016/j.physletb.2015.01.034, arXiv:1409.3392.

[66] CMS Collaboration, "Multiplicity and rapidity dependence of strange hadron production in pp, pPb, and PbPb collisions at the LHC", *Phys. Lett. B* **768** (2017) 103, doi:10.1016/j.physletb.2017.01.075, arXiv:1605.06699.

[67] BESIII Collaboration, "Polarization and entanglement in baryon-antibaryon pair production in electron-positron annihilation", *Nature Phys.* **15** (2019) 631–634, doi:10.1038/s41567-019-0494-8, arXiv:1808.08917.

[68] E877 Collaboration, "Proton and pion production relative to the reaction plane in Au + Au collisions at AGS energies", *Phys. Rev.* **C56** (1997) 3254–3264, doi:10.1103/PhysRevC.56.3254, arXiv:nucl-ex/9707002.

[69] A. M. Poskanzer and S. A. Voloshin, "Methods for analyzing anisotropic flow in relativistic nuclear collisions", *Phys. Rev. C* **58** (1998) 1671, doi:10.1103/PhysRevC.58.1671, arXiv:nucl-ex/9805001.

[70] T. Pierog et al., "EPOS LHC: Test of collective hadronization with data measured at the CERN Large Hadron Collider", *Phys. Rev. C* **92** (2015), no. 3, 034906, doi:10.1103/PhysRevC.92.034906, arXiv:1306.0121.

A Supplemental figures

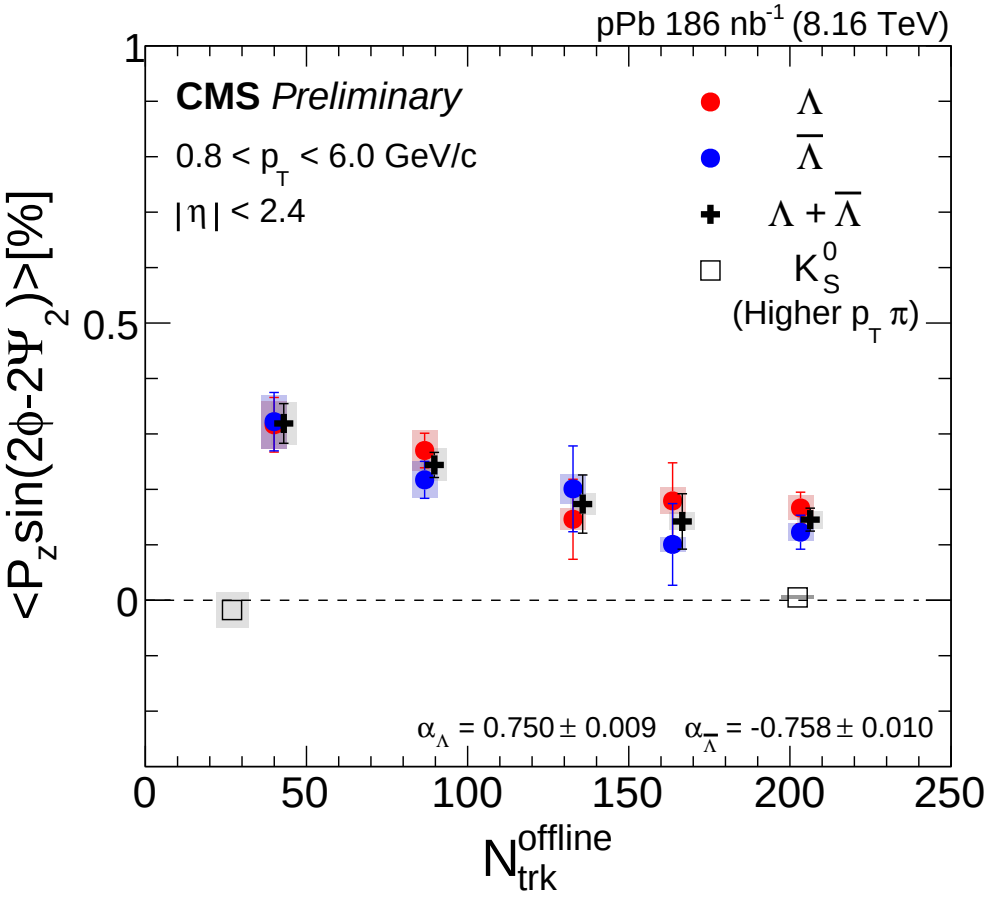

Figure 4: The second-order Fourier sine coefficients of K^0_S, Λ, $\overline{\Lambda}$ and $\Lambda + \overline{\Lambda}$ polarization along the beam direction as functions of $N^{\text{offline}}_{\text{trk}}$ in pPb collisions at $\sqrt{s_{NN}}$= 8.16 TeV. Vertical bars show statistical uncertainties. Shaded areas show systematic uncertainties. The $N^{\text{offline}}_{\text{trk}}$ values of $\Lambda + \overline{\Lambda}$ results are shifted for better visibility.

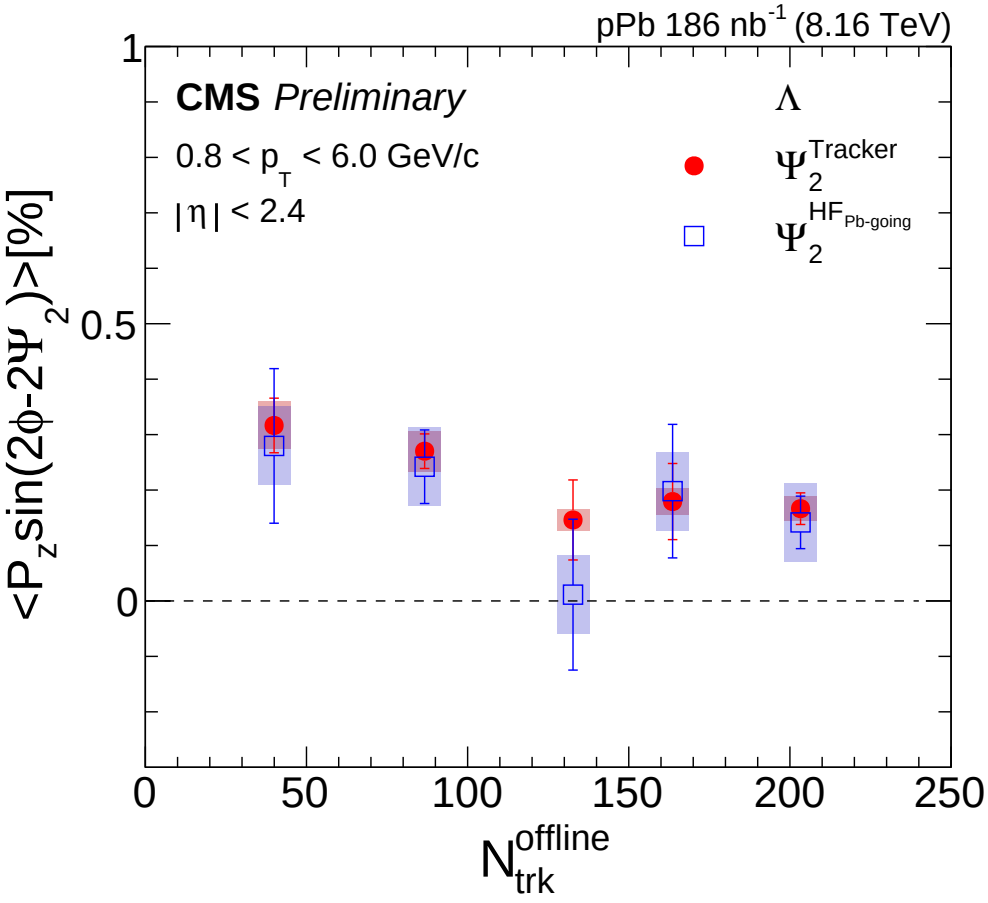

Figure 5: The second-order Fourier sine coefficients of Λ polarization along the beam direction as functions of $N_{\mathrm{trk}}^{\mathrm{offline}}$ in pPb collisions at $\sqrt{s_{_{NN}}}$= 8.16 TeV extracted with tracker and HF event planes. Vertical bars show statistical uncertainties. Shaded areas show systematic uncertainties.

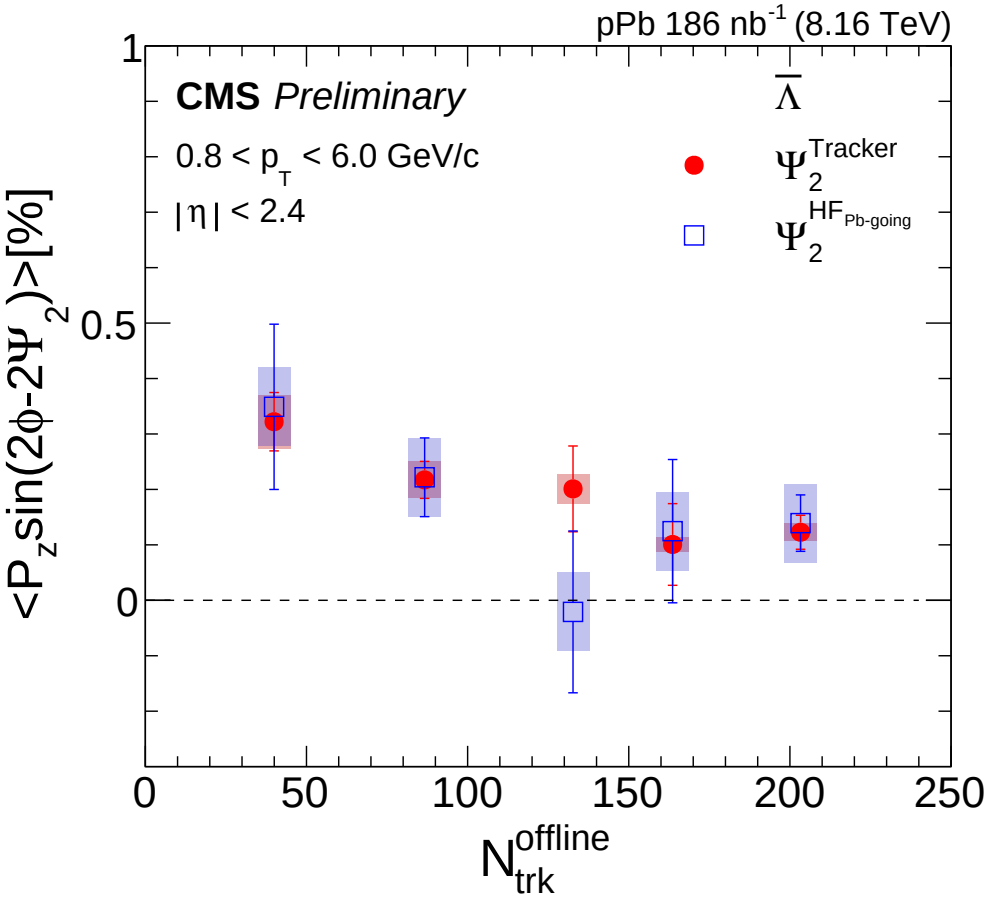

Figure 6: The second-order Fourier sine coefficients of $\overline{\Lambda}$ polarization along the beam direction as functions of $N_{\mathrm{trk}}^{\mathrm{offline}}$ in pPb collisions at $\sqrt{s_{_{NN}}}$= 8.16 TeV extracted with tracker and HF event planes. Vertical bars show statistical uncertainties. Shaded areas show systematic uncertainties.

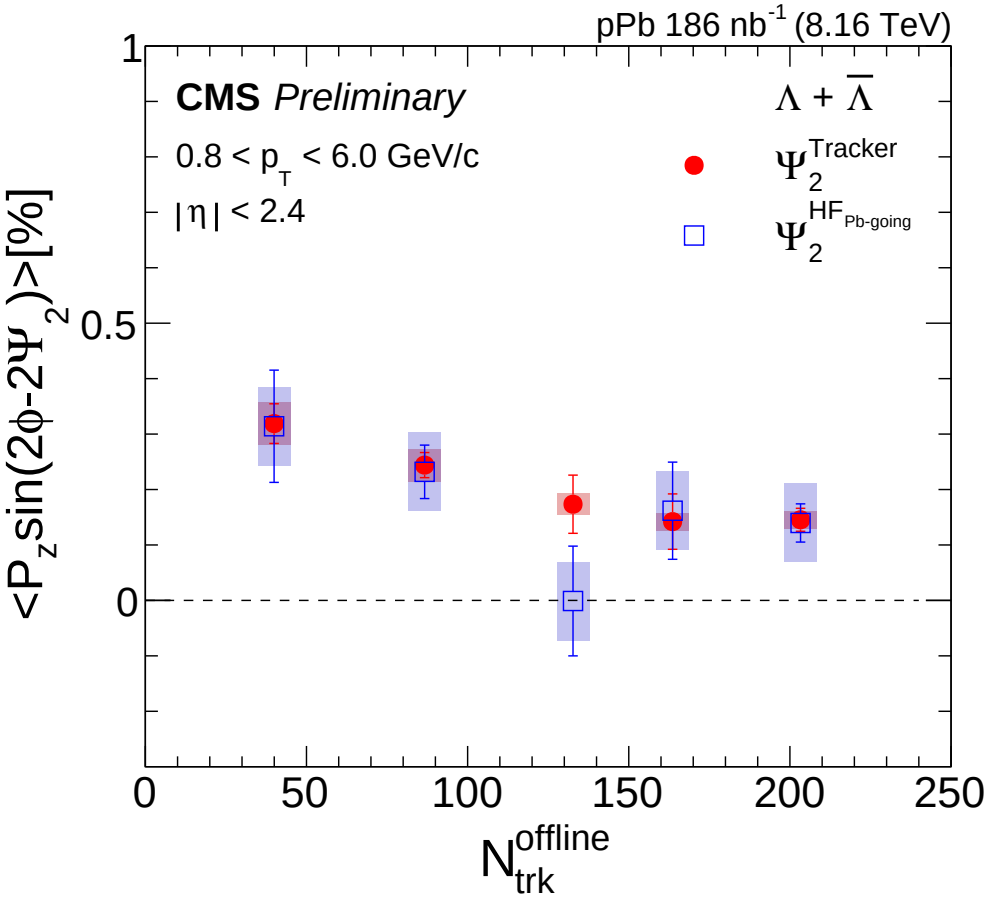

Figure 7: The second-order Fourier sine coefficients of $\Lambda + \overline{\Lambda}$ polarization along the beam direction as functions of $N_{\mathrm{trk}}^{\mathrm{offline}}$ in pPb collisions at $\sqrt{s_{NN}} = 8.16$ TeV extracted with tracker and HF event planes. Vertical bars show statistical uncertainties. Shaded areas show systematic uncertainties.